Wear 584–585 (2026) 206420

Contents lists available at ScienceDirect

Wear

journal homepage: www.elsevier.com/locate/wear

Monitoring the effect of runout on a Diamond-Coated Burrs' wear progression with Acoustic Emission

Thomas Jessel [a,*], Carl Byrne [a], Mark Eaton [a], Ben Merrifield [b], Rhys Pullin [a]

[a] Cardiff School of Engineering, Cardiff University, Cardiff, CF24 3AA, UK
[b] Renishaw plc, Wotton-under-edge, GL12 8JR, UK

ARTICLE INFO

Keywords:
Tool Condition Monitoring
Acoustic emission
Runout
Diamond Coated Burrs

ABSTRACT

Recent Tool Condition Monitoring (TCM) approaches aim to optimise tool replacement by reducing unutilised Remaining Useful Life (RUL) and preventing unexpected failures of Diamond-Coated Burrs (DCBs). Acoustic Emission (AE) has been established as an indirect monitoring method for DCB wear through precision tool measurements. This study assesses the impact of changing initial runout on both wear progression and AE-based monitoring. Twelve wear tests were conducted using an adjustable tool-holder to vary initial runout between 1–78 μm, with AE and frequent on-machine surface measurements collected throughout. Results show that increased initial runout negatively affects total tool life and introduces greater variability in wear behaviour under identical conditions. Using a Renishaw NC4+ Blue (NC4) system, a high frequency of measurements enabled tracking of each DCB's progression through the three wear phases. Surface crater formation and circumferential wear band expansion were consistently observed in the final wear phase of all DCBs. AE proved effective in monitoring both runout severity and the wear progression of the tool's high spot. AE features also identified key wear points throughout the tool's life, regardless of initial runout. These findings highlight the critical influence of runout on small-diameter DCB performance and support AE as a reliable, indirect, on-machine sensing method for tool wear monitoring, capable of identifying varying initial tool conditions.

1. Introduction

Advanced ceramic materials are becoming indispensable within modern industry, a result of their favourable properties for a host of applications [1]. Electronic applications can take advantage of their high operating temperatures, electrical insulation and dielectric properties [2,3], whilst biomedical applications utilise ceramic materials for their high wear and chemical resistance, biocompatibility, and aesthetics [4,5]. In order to obtain the desired dimensional tolerances of complex ceramic components, abrasive machining is required, after sintering [6]. Diamond grinding wheels are employed to combat the high hardness of sintered ceramics, and even then significant machining time is needed, leading the finishing process to incur between 60–95% of the overall manufacturing costs [7]. Additionally, as the final step in the production chain, component damage occurring in this phase is costly [8,9]. As a result, the development of a reliable and accurate TCM approach has been a high priority because of the increased demand for ceramic components and the importance of the abrasive machining phase. With the aim of a developed TCM approach to reduce both the wastage from underutilised tools and damage to ceramic workpieces from unexpected tool failures [10,11].

DCBs are mono-layer, nickel diamond (Ni-diamond) mill-grinding tools capable of manufacturing components from difficult to machine materials. The nature of metal bond grinding tools and the cost-effective electroplating process presents them as the ideal choice within modern mass manufacturing [12]. These tools consist of a single layer of superabrasive grains (diamonds) mechanically held onto a steel shank by an electroplated bond layer (nickel) [1], which enables their use for the precise machining of hard ceramics even at small scales. Fig. 1 shows a radial slice from a micro-CT scan of an unused DCB, in which the layered composition can be identified. A by-product of both their use at small scales, commonly employing DCBs with a diameter of <5 mm, and mono-layer composition is the relatively low number of grains present on a DCB's surface, resulting in inconsistent wear rates and difficult to predict failure points [13].

In the interest of preserving the single abrasive layer, electroplated wheels are not commonly dressed [14], which gives rise to both advantages and disadvantages. The removed requirement of dressing dramatically increases the usability of DCBs, enabling them to be used in non-grinding specific machine tools and dramatically reducing the associated costs and downtime required for the dressing of traditional

* Corresponding author.
E-mail address: jesselt@cardiff.ac.uk (T. Jessel).

https://doi.org/10.1016/j.wear.2025.206420
Received 23 June 2025; Received in revised form 6 October 2025; Accepted 12 November 2025
Available online 21 November 2025

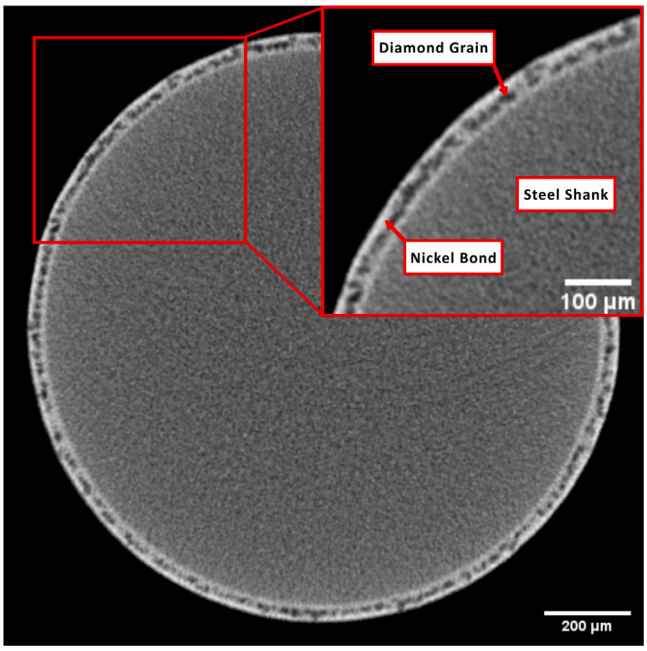

Fig. 1. Radial cross-section of a new ⌀1.3 mm #1000 DCB from a micro-CT scan.

grinding wheels [1,12]. A consequence of this, however, is the inability to correct the grinding tool's form, minimise runout or condition the surface to remove excess bond material and workpiece build-up [14]. A tool's runout describes the error between its geometric centre and its rotational centre. Formed of two terms, axial offset and tilt, runout is the summation of multiple sources of deviation between the tool, tool-holder and machine spindle. Common causes of runout include the clamping of the tool within its tool-holder, inaccuracy during tooling manufacture and poor mating of the tapered contacts [15,16]. Additionally, electroplated tools experience another source of runout stemming from the plating process, whereby there is a potential for non-uniform distribution of the abrasive layer around the tool's circumference [17]. The runout of grinding wheels as with all tooling should be minimised, when unmanaged runout can lead to uneven wear around a tool's circumference, poor surface quality as a result of chatter and in extreme cases complete wheel failure due to uneven stress distributions [18,19]. These adverse effects are more prevalent as the size of the tool decreases, especially as the runout can be larger than the programmed radial depth of cut for a given grinding pass [18,20].

A key aspect of this work is the variation and measurement of runout for small diameter grinding wheels. Diez et al. [16] used an adjustable boring head to vary the runout of a ⌀12 mm fluted end mill, allowing the tool's runout to be varied from 0–40 µm. A dial indicator was utilised to measure the true runout level of the tool between its cutting edges prior to grinding. Badger et al. [19] added runout back to a dressed large diameter vitrified-bond grinding wheel by remounting the wheel on the machine spindle. Through dial indicator measurements around the tool's circumference, an increase in runout from 0 µm to 81 µm was introduced. This method allowed for runout to be investigated via a realistic scenario without any additional equipment, however it limited the author's ability to set a specific value of runout. Similarly to the measurement of micro-milling tools, the runout should not be measured from the tool's shank as there is a machined taper down to the working diameter which can be an additional source of runout [21]. Therefore, measurement of runout for DCBs should be conducted over the grinding surface, to avoid errors from the runout introduced through the taper and electroplating process.

Recently, the development of advanced indirect TCM approaches has been investigated thoroughly. A multitude of sensing methods have been employed to indirectly determine a grinding tool's wear progression and grinding effectiveness, including grinding force [22–24], spindle power [25–27], vibration [28,29], audible acoustics [30] and AE [11,31,32]. Of all the indirect methods AE has shown the most promise to enable a viable on-machine TCM solution [33].

Huang et al. [34] demonstrated the ability of AE to determine a DCB's tool state when grinding a zirconia ceramic workpiece. An ultra-depth-of-field microscope was used to obtain direct measurements of the tool's state, alongside an optical profilometer and electron microscope to analyse the workpiece surface. Transitions between wear phases were identified via abrasive grain fracture and eventually pull-out, with clear differences in grinding mechanisms seen through the workpiece morphology. Both AE amplitude and the wavelet packet energy correlated well with the tool's increasing wear, with power levels varying across the frequency spectrum as different wear mechanisms become more prevalent. Liu et al. [35] showed similar results through both time and frequency AE features, when using a DCB to grind a C/SiC composite. Strong correlation between AE time domain features, such as standard deviation, were identified. However, AE_{RMS} was used as a wear metric in-place of direct tool wear measurements, and a limited number of passes, 90 in total, were completed. Nonetheless, a classification model was trained to predict the tool's wear state, leading to an accuracy of 96% across the small dataset. In a previous publication by the authors [36], the development of an AE based TCM approach was developed through the application of a LSTM regression model. With an increased frequency of on-machine 2D tool wear measurements, a regression model was trained to predict the DCB's radius from AE input features, leading to a mean squared error of 0.550 µm when predicting on unseen data. However, a limitation of all the presented previous works is the lack of consideration of changing initial conditions or validation through a statistically significant number of wear tests. As a result, it is unknown whether these methods could be utilised in real-life manufacturing.

This work details the impact of a DCB's runout on both its total useable life as well as the mechanisms of wear, through conducting a series of wear tests with DCBs at levels of increasing runout. Using a novel methodology, frequent on-machine 3D surface scans of the DCB were collected during each wear test using a NC4 laser tool setter, in contrast to previous works utilising only 2D surface scans. Through these measurements, the progression of wear was investigated and key mechanisms identified. Additionally, AE an indirect and non-destructive sensing technique was utilised to acquire data throughout each wear test, leading to the validation of a passive and time efficient method of monitoring a DCB's runout and wear progression.

2. Methods

Wear tests were conducted with the aim of taking a new DCB to failure to investigate the effect of initial runout on its overall life. Each tool's runout was initially set by using a NIKKEN BT30-SZF10-90 zero-fit tool holder [37] and then subject to a series of repetitive grinding operations, accelerating the normal wear process. During each wear test, both measures of the grinding process (AE) and the tool's wear state, were taken frequently. Each cycle of the wear test comprised of two phases: a grinding phase and an inspection phase. The wear test continues through cycles until reaching the tool's failure point, as shown in the flowchart in Fig. 2. Failure of the tested DCBs was defined as a reduction in the tool's length by ≥0.5 mm. This definition allowed the automatic stopping of a test due to complete failure of a DCB, preventing machine tool crashes, whilst ensuring the final grinding passes of a DCB's life were captured.

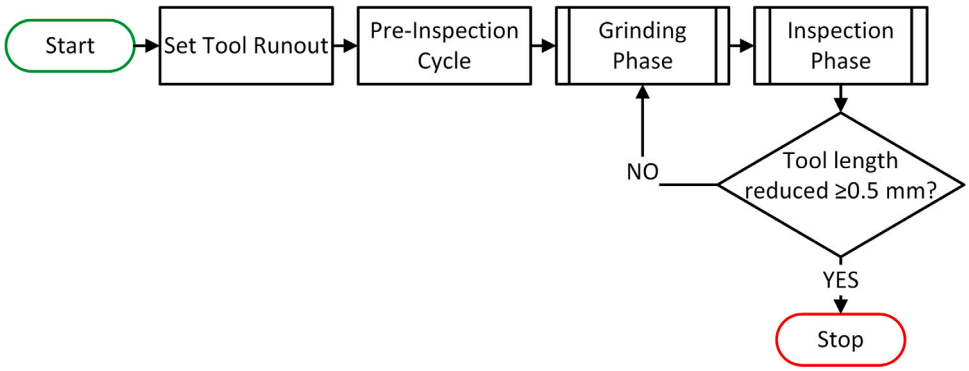

Fig. 2. Flowchart of the wear test procedure.

2.1. Tool setup

In order to observe the effect of runout on a DCB's wear progression, a specialised tool holder was utilised to adjust the DCB's runout into the desired range prior to conducting each wear test. NIKKEN zero-fit tool holders are commonly employed to reduce a given tool's runout. An inbuilt cam allows for a variable force to be applied to a given region of a tool's circumference, which, when aligned with the tool's radial high spot, reduces the overall runout. To carry out this reduction on a typical machining tool, i.e a fluted end mill, a dial indicator is used on the tool's shank to identify the severity of runout and also determine the radial high spot location. In this application, however, the effect of both reduced and increased levels of runout were of interest and as such the runout was increased by applying the cam's adjustment to the radial low spot of the tool's circumference.

To obtain an accurate value for a DCB's runout measurement, a dial indicator was not applicable, due to the small tool diameter and concern for damaging the indicator tip. As such, the NC4 was used to measure 2D surface measurements at multiple locations along the DCB's length, from which the runout was extracted. The process of measuring 2D scans with the NC4 is detailed in Section 2.3.1. Before each wear test was conducted, the tool's initial runout was adjusted to a pre-determined amount. Three "levels" of runout were chosen to represent the full range of feasible runout values [16,19,38,39]. The first of which adjusted a DCB's initial runout to <15 μm. This range was considered to be a "low" level of runout for a DCB of this specification. The second level of runout, labelled as "medium", set the initial runout to between 25–35 μm. Finally, a "high" level of runout was selected as DCBs set to between 75–80 μm, whereby 80 μm was the maximum value capable of being reached using the NIKKEN zero-fit tool holder.

2.2. Grinding phase

Each wear test utilised a Genentech ⌀1.3 mm #1000 DCB in order to grind a Silicon Carbide (SiC) workpiece. To wear the DCBs a side-milling operation was utilised with consistent grinding parameters for all tests. The grinding phase followed the same methodology as [36], enabling the expansion of an existing dataset. Table 1 shows the grinding phase specification for all conducted wear tests. A schematic of the side-milling operation with the grinding parameters from Table 1 labelled can be seen in Fig. 3.

The grinding phase consisted of a single side-milling pass across the 20 mm width of the workpiece, L, during which AE was recorded continuously. Fig. 4 shows the operation chain during the grinding phase. Prior to each wear test, the SiC workpiece was first re-surfaced flat and parallel to the machine axes. A MISTRAS Wideband Differential (WD) sensor was bonded with Loctite SI 595 silicone sealant to the workpiece's top face, acting as both an acoustic couplant and environmental protection. Alongside a MISTRAS 2/4/6 pre-amplifier, with a gain of 20 dB and an internal bandpass filter of 0–1200 kHz enabled the collection of AE from within the machine tool. Due to the continuous nature of AE produced by any grinding process, a National Instruments (NI) PXI oscilloscope sampling at 2 MHz was used for acquisition of the AE.

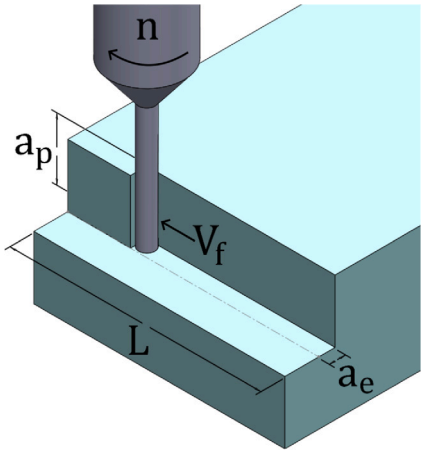

Fig. 3. Schematic of the DCB side-milling operation, with labelled parameters.

2.3. Inspection phase

To relate the acquired AE during the grinding to the resultant tool wear, an on-machine inspection cycle was conducted after every grinding pass using the NC4. The inspection phase comprised of two measurements, a 2D circumferential surface scan at a fixed position and a new to this work, 3D surface scan of the entire tool's length. The 2D circumferential surface scan was conducted after every grinding pass, at a fixed axial position up the tool. Full 3D spiral scan measurements were conducted less frequently, after every fifth grinding pass. However, the 3D NC4 scans were crucial to account for any large changes that occur outside the 2D surface measurement window, gaining a more complete understanding of the tool's wear state. Fig. 5 shows the order of operations during the inspection phase.

2.3.1. NC4 - DCB measurements

A NC4 [40] was used to obtain on-machine tool radius measurements. The NC4 is a non-contact tool setting system that determines the radius of a tool by using it to obscure a laser beam. It consists of a transmitter tower and a receiver tower, housing a sensor used to measure the incident laser power across its face [41]. In a normal radius measurement macro, the NC4 operates through a trigger mode, in which a rotating tool is moved perpendicularly into the laser beam. When the tool blocks the beam sufficiently to reduce the incident power

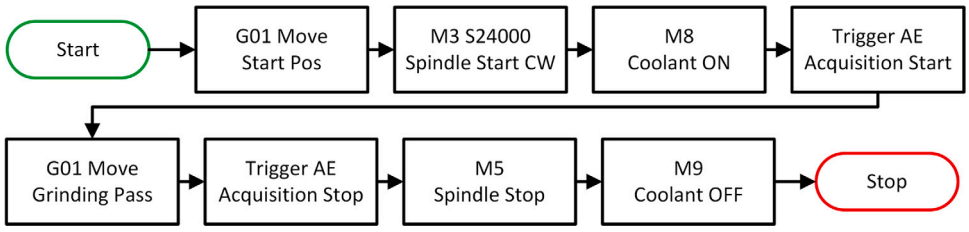

Fig. 4. Flowchart of the grinding phase subprocess.

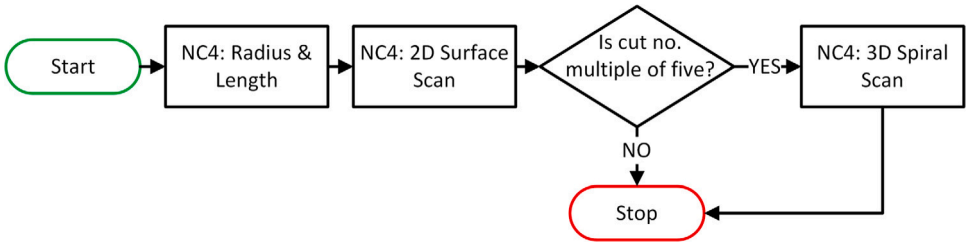

Fig. 5. Flowchart of the inspection phase subprocess.

Table 1
Grinding specification.

Grinding parameters	
Grinding machine	Jingdaio VT600 A12S
Machining operation	Side milling
Spindle speed, n	24 000 rpm
Cutting speed, V_s	98 m/min
Feedrate, V_f	60 mm/min
Depth of cut - Axial, a_p	5 mm
Depth of cut - Radial, a_e	0.03 mm
Grinding length, L	20 mm
DCB specification	
Tool geometry	Cylindrical
Type	Electroplated mono-layer
Tool diameter	ø1.3 mm
Mesh size	#1000
Abrasive grain size	15 µm
Workpiece specification	
Material	Green Silicon Carbide
Bond type	Vitrified
Dimensions	100 × 20 × 10 mm
Grain size	240
Knoop hardness	2840 $kg_f\,mm^{-2}$
Relative toughness	1.6
Coolant specification	
Coolant	Supergrind ultra
Supplier	Morris lubricants
Type	Synthetic water-based
Concentration	2.5–3.0%
Operating temperature	18 °C
Flow rate	4 L min^{-1}

by a preset threshold, typically 50%, a trigger is sent to the machine controller to stop movement. The tool's radius is then calculated from the difference in machine and beam co-ordinates, outputting a single value for the tool radius. Fig. 6 shows a schematic of the NC4 with a representative rotating tool positioned at the 50% radial laser obscuration position. This technique provides a quick but precise average value of the tool's radius, however this is limited for use in TCM approaches by only providing a simplified representation of the tool's wear.

2D surface scan. To provide more information relating to the tool's wear, the NC4 system can be used in an alternative strategy. This approach takes advantage of the concept that the radius of a rotating tool can be measured through the changing incident laser power levels. If a tool is moved so that its edge is within the beam and then rotated but not translating, any change in the measured power level is the result of the beam becoming more or less obstructed, from which the radius of a tool required to block the beam by an equivalent amount can be determined. The transmitter produces a beam which at its centre point, the midpoint between the two towers, is approximately 40 µm in diameter [42], over which the sensor will detect a drop in power if obscured. Through the calibration process of an NC4 a linear function is derived to convert the output sensor voltage into a radius that results in the equivalent beam obstruction. Using an external oscilloscope, the NC4 receiver's voltage can be polled whilst the tool is rotating, to obtain a 2D measurement of the tool's circumferential radius. The same NI PXI oscilloscope used for the capture of AE was used to record the NC4 output voltage at a sample rate of 50 kHz. A spindle of speed of 60 rpm was used to rotate the tool within the beam, resulting in measuring 7958 samples rad^{-1} about the tool's circumference. Fig. 7 shows an example of the converted 2D surface scan.

In every wear test, the 2D surface scans were conducted halfway up the axial depth of cut, a_p (2.5 mm from the end of the tool). By measuring at the same position, this measurement enables the progression of wear to be observed around the tool's circumference. Additionally, from these 2D scans more information other than just mean radius can be extracted, such as maximum radius, runout and form error, all of which provide useful insights to the tool's state and ability to grind effectively.

3D spiral scan. A major downside of the 2D NC4 scans are that circumferential measurements only occur at one axial position up the tool's length. As a result, there is still the possibility of missing large parts of the tool's overall wear, which will still impact both the ground workpiece surface and the produced AE during grinding. Therefore, to obtain a comprehensive view of the wear process, a pseudo 3D scan was implemented. To generate this 3D plot, the tool was both rotated and translated in the Z-axis simultaneously, making the measurement point follow a spiral path up the tool's surface. Through varying the spindle speed and Z-axis feedrate, higher resolution scans can be produced with the penalty of scan time increasing. Fig. 8(a) shows an example of this type of 3D measurement taken of a new ø1.3 mm DCB, in which the tool has been measured from its tip to 7 mm up its length. Each NC4 spiral scan measures from below the tip of the tool (at Z = 0.2 mm) to beyond the axial depth of cut asked of the DCB, showing a clear contrast between the wear of a worn and un-worn section of each DCB. The large protrusion at the tip of the tool above 0.68 mm, highlighted in red in

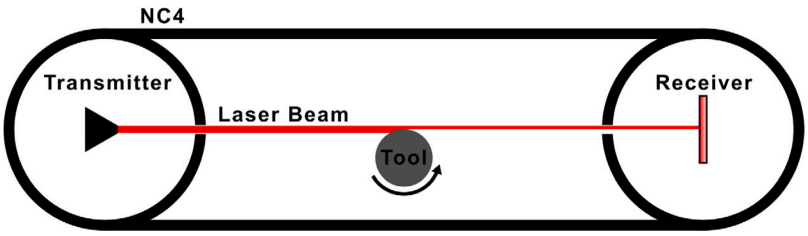

Fig. 6. Schematic of an NC4 with a tool obscuring the laser beam.

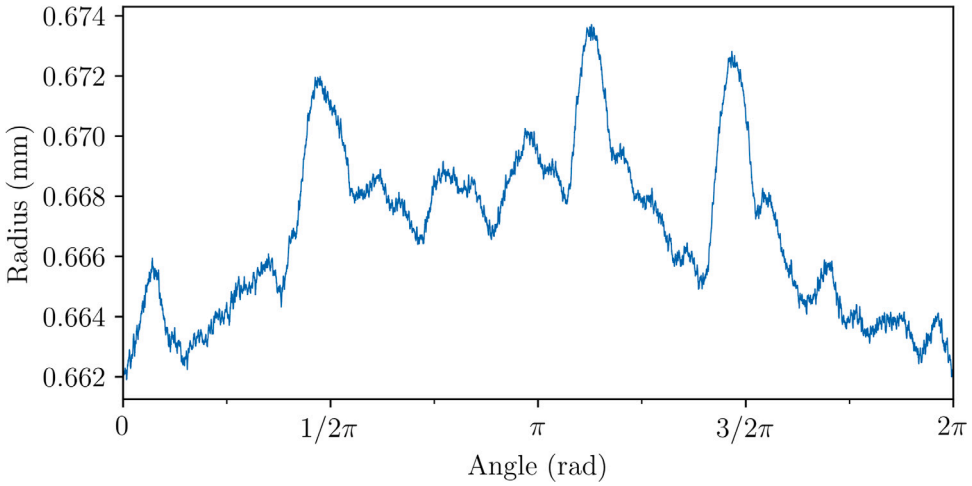

Fig. 7. A processed NC4 - 2D surface scan of a new ⌀1.3 mm #1000 DCB.

Fig. 8(a), is a narrow band of coolant and therefore can be ignored. For comparison, a scan of the same tool after 75 grinding passes is shown in Fig. 8(b), in which the tool's wear can clearly be identified across the grinding region. The area of contact between workpiece and tool is shown by the labelled red box in Fig. 8(b), with regions of significant localised wear forming surface craters also highlighted.

3. Results

Twelve full wear tests were completed in total, in order to observe the effect of differing runout levels on tool wear and overall life. Fig. 9 shows the runout of each DCB prior to each wear test, the colouring of each bar representing the runout level. Six tests were conducted with "low" levels of runout, with three tests being conducted with DCBs in both the "medium" and "high" ranges, previously set out in Section 2.1.

3.1. Runout's effect on tool wear

Throughout the entire wear test series, the only variable was the initial DCB runout, leading variations in total tool life to be the direct result of changing runout levels. The total number of completed grinding passes by each DCB can be seen against the initial runout level in Fig. 10, the figure follows the same colour configuration as in Fig. 9. This scatter plot displays a key insight to the operation of these tools, the variability of a DCB's overall life (i.e. the total number of passes a tool can complete prior to failure) dramatically increases as the level of runout increases. As with all grinding wheels, there will always be some inherent variation in grinding life due to the random nature of grain distribution during manufacture, which can be seen within the wear tests conducted at the "low" runout range exhibiting a range of 16 passes. Whereby, the three wear tests conducted within the "high" runout range resulted in a range of 99 passes. This increase in unpredictability of a grinding wheel's life is a major concern when considering that these tools are normally used within machines without in-process tool measurements at the mass-manufacturing scale. Without the evaluation and consideration of a DCB's runout level, it is very difficult to implement any basic tool replacement strategy. However, by comparison, a DCB that has had its runout adjusted to <15 μm leads to a much reduced range in tool life, enabling a simple confidence interval method to be employed as a DCB replacement strategy without excessive wastage. Additionally, taking a DCB from the "medium" to "low" region of runout, a decrease in runout of 20 μm, results in an increase to the total number of passes a DCB completes by 39%. Knowledge of the DCB's runout level is crucial, even when the runout cannot be removed in-situ, as it allows the controller to make a more informed prediction on the DCB's useable life.

Both the increased variability and decrease in overall life of DCBs resulting from increasing levels of runout can be explained by looking at the mechanism of wear progression. Figs. 11 and 12 show three NC4 spiral scans of the DCB used during tests 4 and 10 respectively, each having been measured 20 grinding passes apart from one another. The DCB used in test 4 exhibited the second lowest initial runout of all the conducted wear tests (2.71 μm), whilst in test 10 the DCB had a measured initial runout of 76.05 μm. The two figures show stark differences in overall wear and contact regions.

Fig. 11(a) shows the DCB's wear after completing 80 grinding passes, (58% through its total life). Its overall wear is significant, having been reduced on average by 14 μm, through a comparison of the worn and unworn sections of the DCB's length in the figure. As a result of the DCB's low runout the tool is capable of sharing the grinding load across the entire surface of abrasive grains. Leading to the progression of wear to be consistent around the tool's circumference. After another 20 passes, the wear has progressed and small isolated areas of the DCB's surface have worn beyond the mean surface, forming surface craters seen by the dark blue areas on Fig. 11(b), indicating a loss of abrasive grains within those regions. Surface craters are the result of individual regions of the tool wearing faster than the surrounding surface, the location and severity of which stem from the random distribution of grains on a DCB's surface. Once formed, a surface crater will

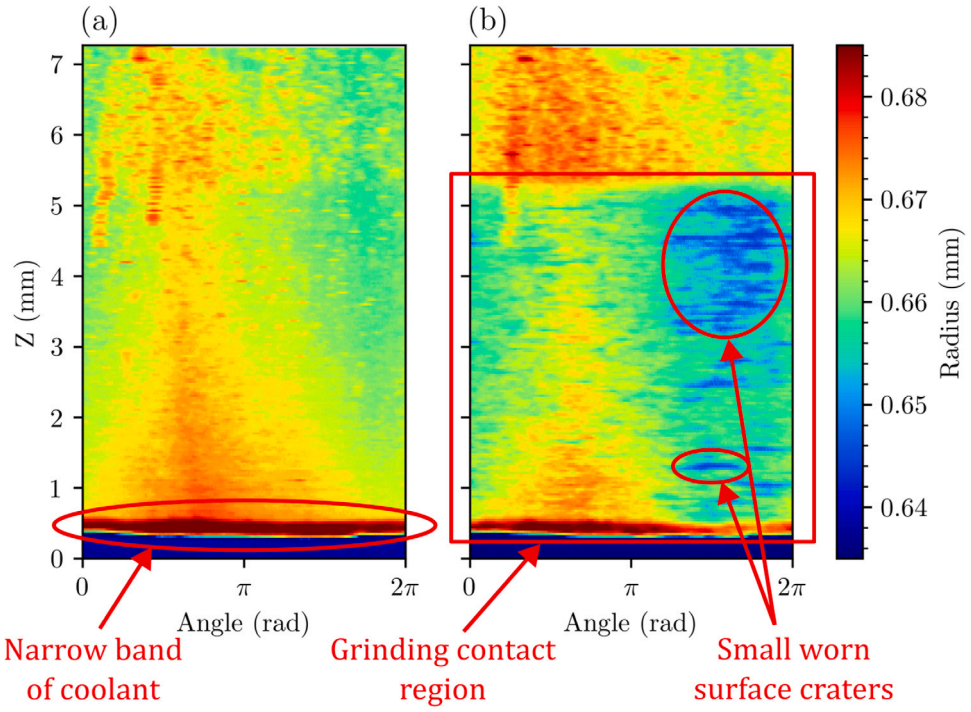

Fig. 8. 3D NC4 spiral scans of a ⌀1.3 mm #1000 DCB after (a) zero and (b) 75 grinding passes. With red labels and text showing prominent features. (For interpretation of the references to colour in this figure legend, the reader is referred to the web version of this article.)

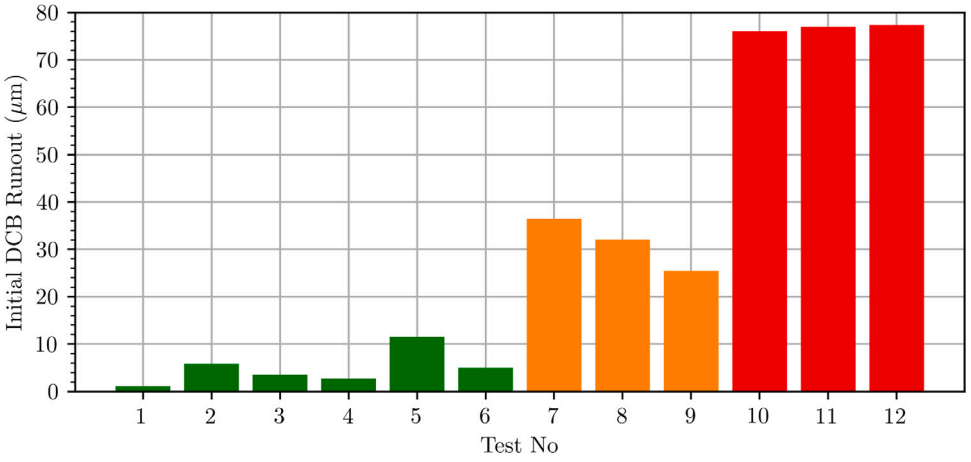

Fig. 9. The initial DCB runout set prior to each wear test. (For interpretation of the references to colour in this figure legend, the reader is referred to the web version of this article.)

expand radially, a result of the grinding load no longer being equally distributed around the DCB's circumference, leading to bands along the tool's length that are entirely void of abrasive grains. This mechanism can be seen in Fig. 11(c) whereby bands of wear have formed from the existing crater locations, in which the entire Ni-diamond layer has been removed around the tool's circumference. Once a band has formed, it quickly increases in width along the DCB's length, leading to tool failure. The formation of craters and later bands is present in all wear tests conducted at lower runout levels.

In contrast, Fig. 12(a) shows that the DCB during test 10 has a large high spot, a consequence of the "high" runout, encompassing roughly a third of the DCB's circumference. Due to the runout and changing level of grain penetration, there is a large variation in grinding load for any given abrasive grain on the tool's surface. This difference in contact impacts the progression of wear around the tool's circumference. Consequently, the wear during test 10 occurs solely across the current high spot, at an increased rate due to the reduced contact area and higher grinding loads. This can be seen in Fig. 12(b) by the wear having first been removed across the high spot and leaving a crater along the tool's length, which in Fig. 12(c) continues to wear and expand around the tool's circumference as the new high spots are worn away. The same mechanism of crater and banding formation is present for DCB's operating at high runout levels, however the random grain distribution plays a much larger role in determining the tool's overall life. The density of abrasive grains across the DCB's surface and adhesive strength between the Ni and diamond grains varies as a result of the electroplating process. This leads to regions of the DCB's surface being more or less resistant to the formation of surface craters. With increasing DCB runout this variation in wear resistance becomes more critical, as it relies on a smaller region of the abrasive layer distributing an increased grinding load. Therefore, DCBs operating at higher runout levels have an increased variance in overall tool life, a result

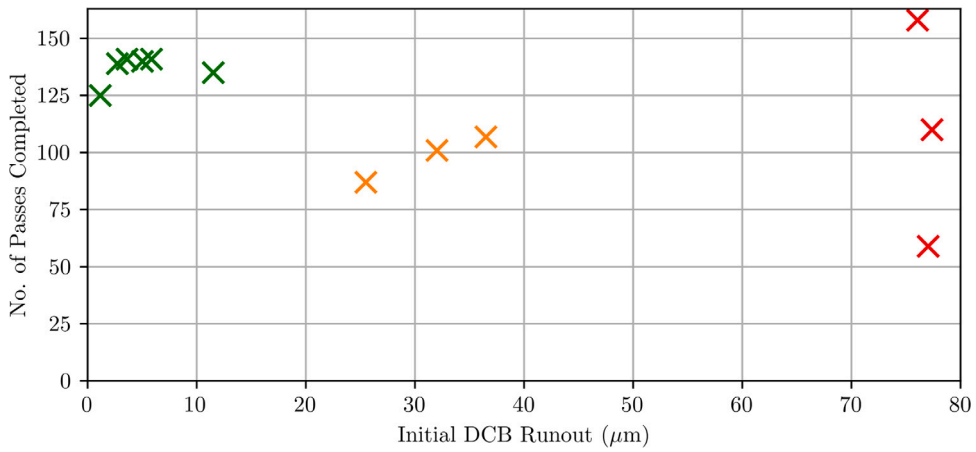

Fig. 10. Total number of grinding passes completed by each wear test against each DCB's initial runout. (For interpretation of the references to colour in this figure legend, the reader is referred to the web version of this article.)

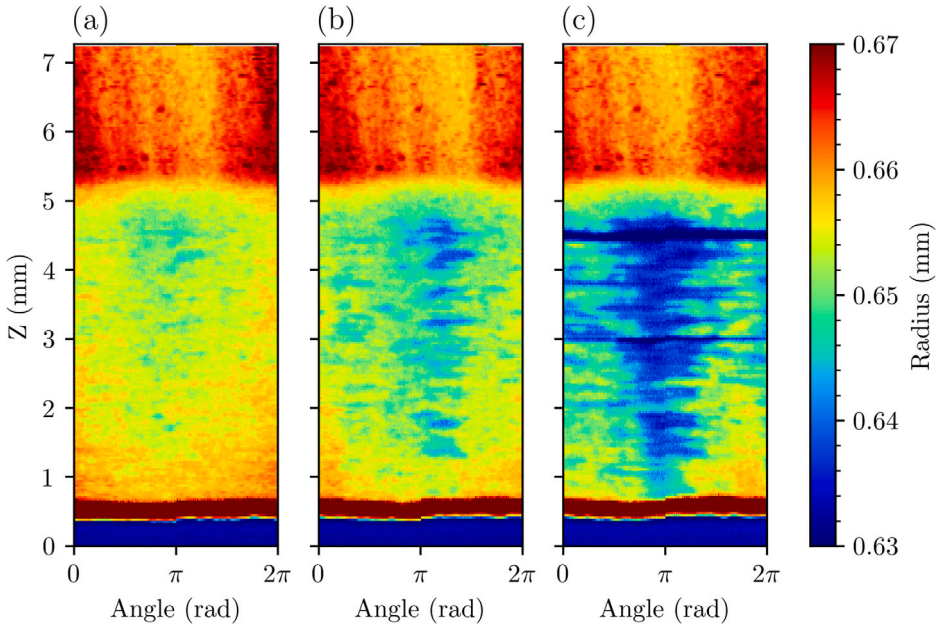

Fig. 11. NC4 spiral scans of the DCB from test 4 after (a) 80 passes, (b) 100 passes and (c) 120 passes. (For interpretation of the references to colour in this figure legend, the reader is referred to the web version of this article.)

of their initial high spot's resistance to crater formation. Conversely, a DCB operating at a lower runout level, is capable of distributing the grinding load across a larger contact area, and therefore more abrasive grains. Allowing even weaker regions of the DCB's surface to resist the formation of wear bands until the majority of the abrasive layer has been worn.

Fig. 13 shows the 2D NC4 circumferential scans and extracted wear metrics, throughout test 4. Fig. 13(a) shows each NC4 2D scan after alignment, through which the wear of high spots and formation of craters on the DCB's surface can be seen. From this data, the mean and peak radius were extracted, shown below in Fig. 13(b). The three phases of tool wear (initial wear-in, steady-state and wear-out) can be identified through the observation of the gradients of both metrics in Fig. 13(b).

The initial wear-in phase is characterised by a short period of high wear rate, usually lasting <10 passes, during which weakly adhered grains and any superfluous Ni bond material covering the abrasive layer are quickly removed. This can be identified in Fig. 13 by the rapid initial wear rate across the first six grinding passes, whereby all high spots above 0.67 mm radius are removed.

The wear rate will start to slow as an increasing number of grains are exposed, reducing the overall grinding stress asked of each abrasive grain. Thereby leading into a period of steady-state wear, during which the single layer of abrasive grains are slowly worn away. When grinding with adequate and reasonable parameters, this phase covers the majority of the DCB's life, seen in Fig. 13(b) by the relatively constant gradient across grinding passes 6–121. During this phase, abrasive grains are worn or pulled out of the bond material, slowly reducing the grinding capability of the DCB. The wear rate is slowed by grains re-sharpening through micro-fracture or their load further shared by other newly exposed grains, however once exhausted the DCB will wear rapidly into the bond material. This effect can be seen in Fig. 13(a) whereby small craters around the tool's circumference are worn below the mean height of the surface around grinding pass 40, without any impact on the DCB's ability to grind. However, after 80 cuts further craters develop below the abrasive layer, 0.64 mm radius, at which point the Ni bond material and steel core are exposed.

After forming craters through the abrasive layers, the grains held on either side are required to remove a greater proportion of the programmed radial depth of cut, a_e, on any given rotation, leading to

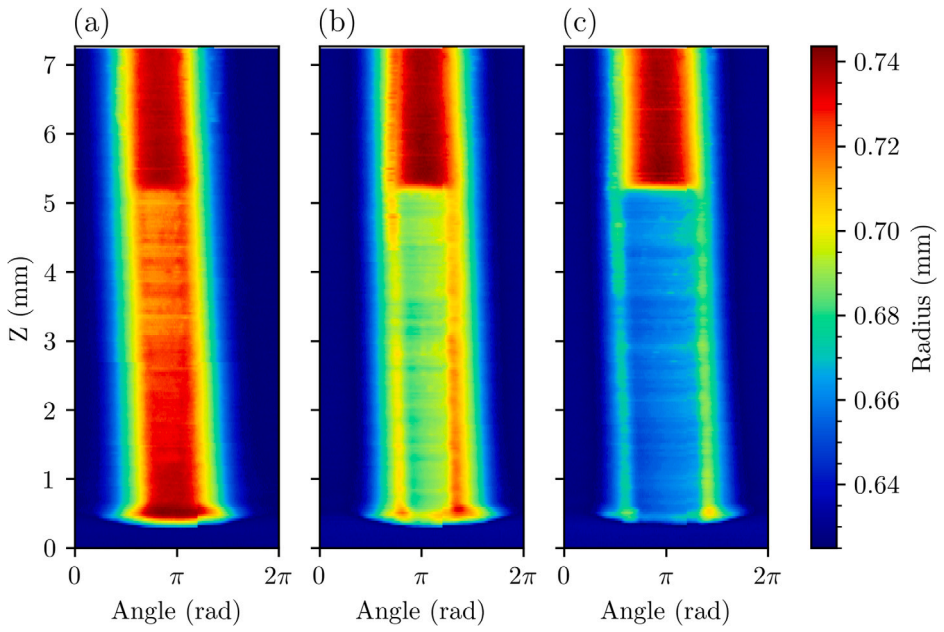

Fig. 12. NC4 spiral scans of the DCB from test 10 after (a) 60 passes, (b) 80 passes and (c) 100 passes.

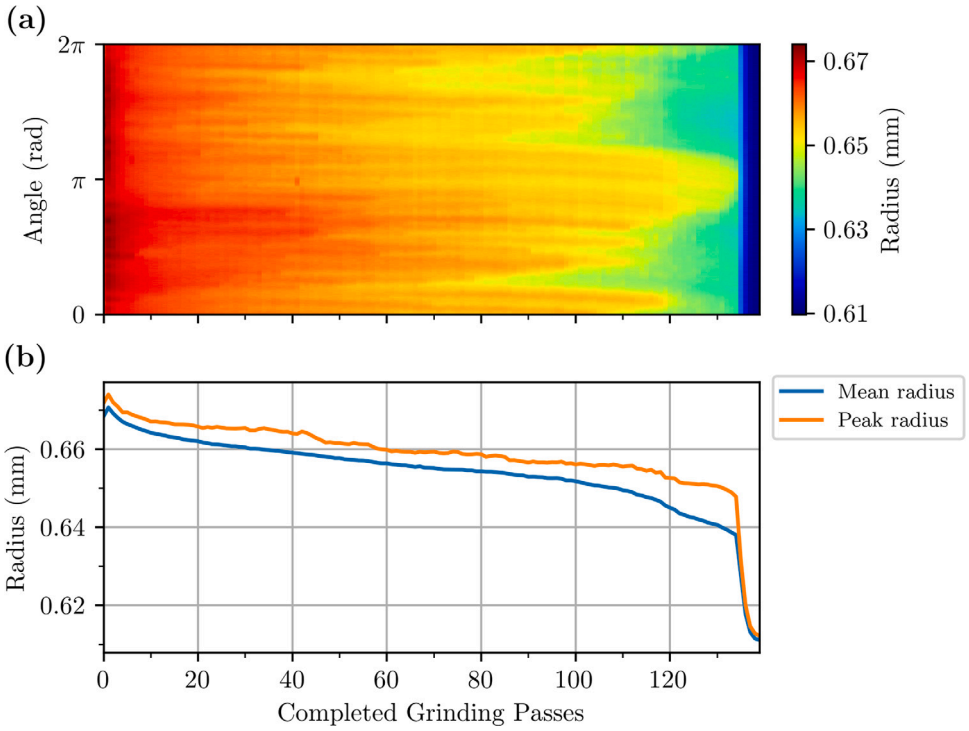

Fig. 13. DCB wear measurements during test 4: (a) NC4 2D circumferential scans, (b) Extracted DCB radius measurements.

the expansion of the formed channels around the DCB's circumference. At a certain point, the number of abrasive grains present on the tool is insufficient to remove the a_e from the workpiece, at which point the workpiece starts grinding the tool instead. This leads to a dramatic increase in wear rate, due to the hardness of the SiC workpiece being much greater than the remaining Ni and steel core, eventually resulting in total DCB failure. The start of this period, called wear-out, can be observed in Fig. 13(a) by the formation of deep craters below 0.64 mm covering the majority of the DCB's surface after pass 122. After the wear of the final region of abrasive grains, centred at 3.14 rad, the wear rate rapidly increases, seen in Fig. 13(b) after grinding pass 135.

The same measurements for the DCB used during test 10 can be seen in Fig. 14. Similarly to Fig. 12, Fig. 14(a) shows a large high spot encompassing a third of the DCB's circumference. After 60 grinding passes have been completed, the high spot starts wearing through its peak, leading to a large crater developing in its place. As the crater develops, two distinct surface peaks become exposed, seen in Fig. 14(a) by the forked shape, which then wear and expand to encompass the whole DCB's circumference. Due to the high runout of the tool, Fig. 14(b) shows a trend unlike a traditional tool wear curve. As the DCB's runout, 76.05 µm, is significantly larger than the a_e, 30 µm, the DCB only makes contact with the workpiece across its highest points. This

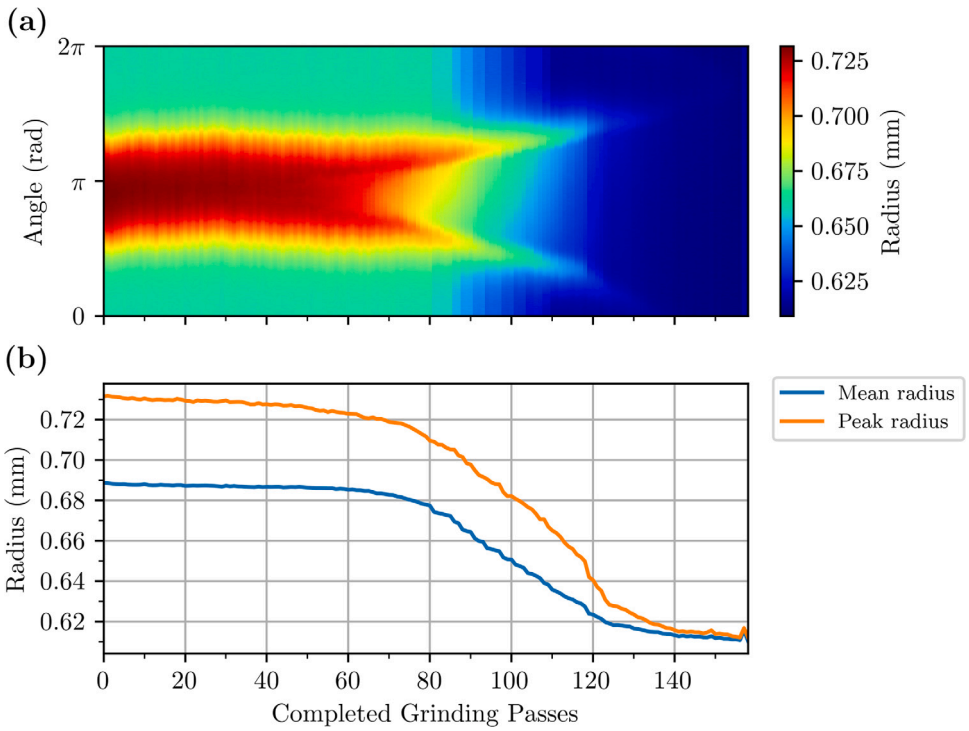

Fig. 14. DCB wear measurements during test 10: **(a)** NC4 2D circumferential scans, **(b)** Extracted DCB radius measurements.

reduced contact region results in the rest of the DCB's circumference experiencing a delayed wear-in phase. Therefore, the traditional wear-in phase occurs over less grinding passes, and has no noticeable effect on the mean radius of the tool, as can be seen in Fig. 14(b). The same effect, of only a fraction of the tool being in contact, also leads to a drawn out wear-out phase. As the highest spots are starting to experience wear-out, other sections of the tool are being brought into contact and therefore experiencing wear-in, explaining the gradient of wear between passes 80–120 in Fig. 14(b).

The same pattern of wear and results can be seen to a lesser extent in Fig. 15, which shows the wear measurements during test 8. Due to the reduced level of runout in test 8 compared with test 10, Fig. 15(b) shows a more typical wear curve with clear wear phase transitions. However, the impact of runout can still be seen as the once the DCB's high spot wears, it forms two distinct surface peaks that slowly wear around the tool's circumference.

Both the 2D and 3D NC4 scans show how the DCB wear mechanism changes with increasing runout. The reduced contact regions between the DCB and the SiC workpiece, when running at a "high" level of runout, lead to the tool's overall life being harder to predict without direct or in-direct tool measurement techniques. The NC4 is a capable direct technique that not only can measure the DCB's runout, but also monitor its overall wear progression. Identification of crater formation and wear band expansion, the main indicators of large scale wear, can both be clearly seen through the use of a NC4 system. However, the collection of these measurements are costly, the time taken to collect a 3D, 2D and 1D NC4 measurements are roughly 4 min, 1 min and 30 s respectively. Leading to a significant amount of downtime, compared to the grinding pass that lasts 20 s. As such, an indirect method capable of inferring the same information without the associated downtime is an ideal solution.

3.2. Acoustic emission

Continuous AE was acquired during each grinding pass, leading to 1443 AE signals being collected, each of which lasting over 20 s. Fig. 16(a) shows the full time-domain AE signal from the 25th grinding pass of test 5. In which the contact period, when the DCB is in contact with the workpiece, can be seen through the large increase in amplitude between 0.8–20.5 s. From Fig. 16(a) the grinding seems to be a continuous high-amplitude AE signal throughout the entire contact period. Fig. 16(b) shows a zoomed in section of the same signal, between 5.00–5.025 s which presents a different view. Whilst the signal is still continuous in nature, indicated by the grinding never allowing the signal to return to the noise floor, the amplitude is clearly pulsing at a consistent frequency. The observed oscillation has a frequency of 400 Hz, with its peak occurring every 2.5 ms, inline with the rotational speed of the DCB, 24 000 rpm. Due to the random distribution of grains on a tool's surface, a tool with zero runout and a perfect circular form should produce a consistent level of AE, therefore the observed pulsing pattern is a consequence of the tool reducing in contact as it rotates.

Validation of this can be seen in Fig. 17, in which a 10 ms section of AE has been extracted from the 10th pass of tests (a) 6, (b) 9 and (c) 12. The associated DCB's runout level after each respective pass were 7.15 µm, 24.97 µm and 75.25 µm. The effect of increasing runout, and as a result decreasing the proportion of tool-workpiece contact per revolution, can be seen in Fig. 17. In tests 9 and 12, as the DCB breaks contact with the workpiece during a revolution, it allows the AE to ringdown to the noise floor. Both the time the AE remains above the noise floor and the rate at which the AE decays, indicating the severity of the DCB's runout.

Figs. 18–20 show the aligned AE power envelopes from a single DCB revolution during each grinding pass of tests 4, 8 and 10 respectively [43]. From which the AE source location can be placed around the DCB's circumference. Fig. 18 shows a consistent level of AE power both throughout the DCB's life and around its circumference, indicating the grinding process is also constant in its aggressiveness. This results from the DCB in test 4 having a "low" level of runout, initially 2.71 µm, in which the entire tool's surface will make contact throughout a revolution. Additionally, in the figure, the wear-in phase can be identified through increasing power levels and contact area within the first six passes.

Figs. 19 and 20 show a different pattern of AE power as a result of the high spot present on each DCB's surface. In each, a clear portion

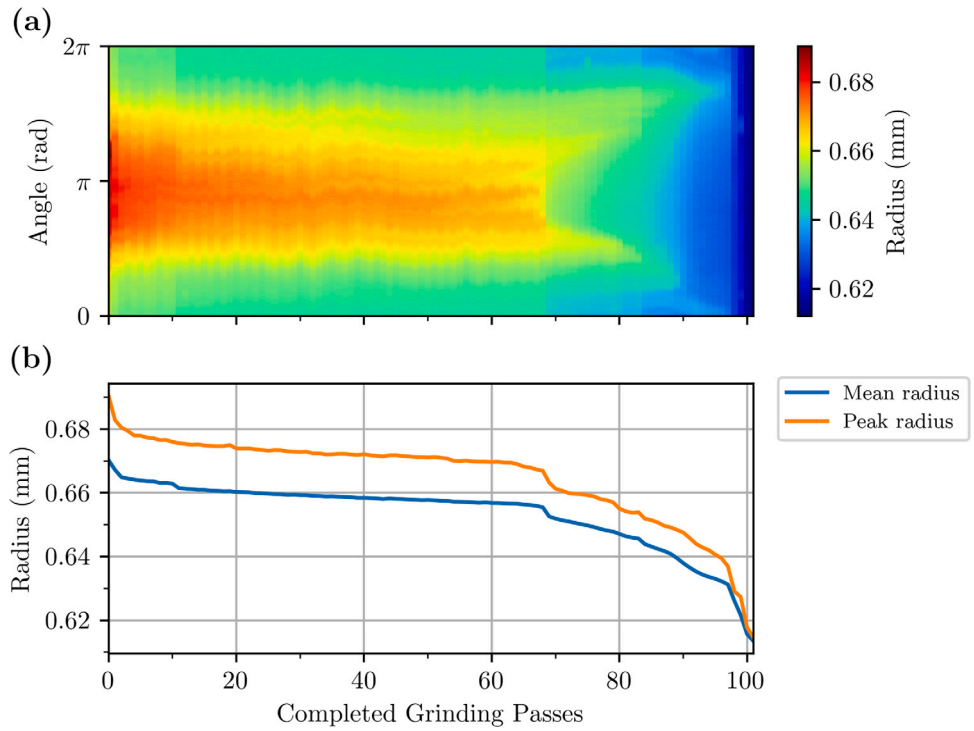

Fig. 15. DCB wear measurements during test 8: **(a)** NC4 2D circumferential scans, **(b)** Extracted DCB radius measurements.

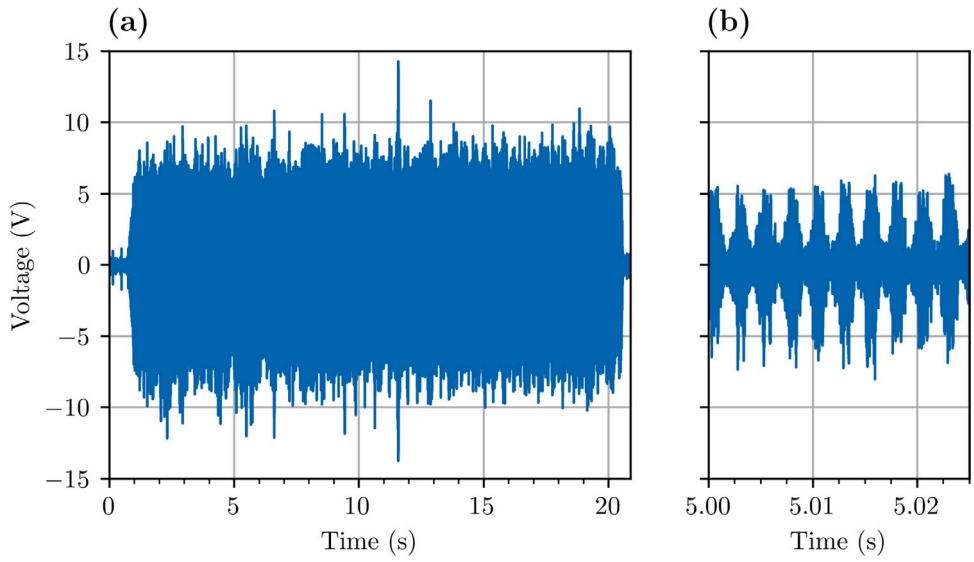

Fig. 16. Time domain AE signal acquired during the 25th pass of test 5 showing the (a) full signal and a (b) zoomed in section.

of the DCB's circumference is generating a large amount of AE power, indicative of the tool only making contact with the workpiece over these portions. Outside this region of high AE power and tool-workpiece contact, the following drop in power results in a lower baseline during test 10 shown in Fig. 20, falling below 50 dB, additionally the contact region occurs over a smaller proportion of the DCB's circumference, both of which indicate a higher level of runout when compared to test 8. The creation and expansion of wear craters can be seen in both Figs. 19 and 20. At grinding pass 65 and 70 respectively, the regions of high AE power split into two individual peaks, aligning with when the high spot initially wears away on the DCB, observed in Figs. 14 and 15. The peaks slowly increase in separation around the tool's circumference, at which point they rejoin prior to the failure point. This aligns with the wear measurements seen during both test 8 and 10, in Figs. 14 and 15, whereby a crater formed at the high spot slowly expands to encompass the entire circumference.

3.2.1. Extracted AE features

The raw time-domain AE signals are capable of identifying the contact period between the DCB and the SiC workpiece, indicating the level of runout a tool has and capable of visualising the progression of wear around a tool's circumference. However, due to the scale of the acquired data and required computing power to process it, AE is typically abstracted into simplified features that represent the raw time-domain signals. Both the AE_{kurt} and AE_{RMS} are useful metrics for determining the grinding condition and aggressiveness indirectly [43]. Figs. 21 and 22 show the respective AE features throughout tests 4, 8

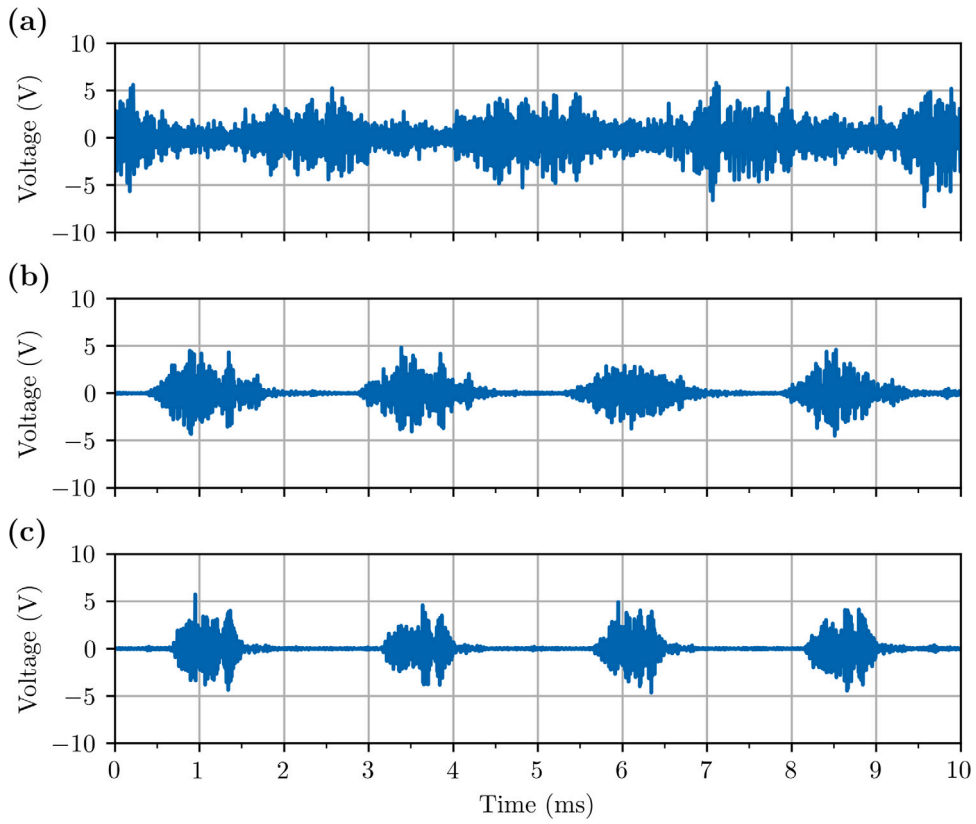

Fig. 17. An example AE signal from three separate tests with increasing DCB runout; **(a)** Test 6, **(b)** Test 9 and **(c)** Test 12.

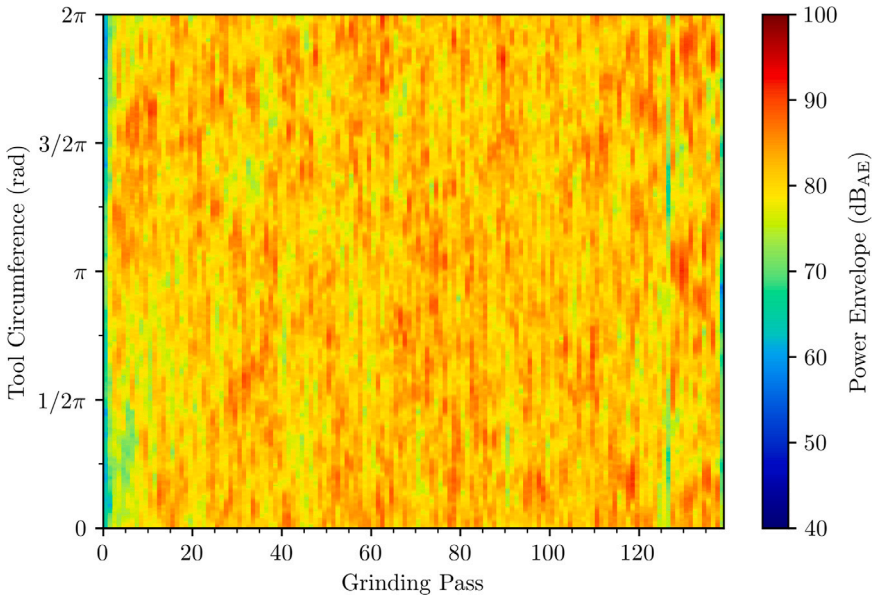

Fig. 18. AE power envelope from a single tool revolution of every grinding pass during test 4.

and 10, with the other wear tests in each runout range not presented but following similar trends.

AE_{kurt} represents the "tailedness" of an AE signal's distribution, which when applied to continuous AE indicates the proportion of the signal occurring at its maximum absolute voltage. The idealised DCB producing a consistent level of continuous AE throughout its life will result in a normal distribution of AE, and therefore a low AE_{kurt} of three. However, as seen in Fig. 17(a) even low levels of runout leads to variation in the generation of AE as a DCB rotates, due to the reduction in contact with the workpiece. Explaining why the AE_{kurt} of test 4 is slightly above three throughout its steady state phase in Fig. 22. Furthermore, the increasing level of runout used in tests 8 and 10 results in clear increases in the level of AE_{kurt}, a consequence of the decreasing level of tool-workpiece contact.

During the wear-in phase of each test, the AE_{kurt} starts off high and drops to a baseline level. After reaching this baseline level, the AE_{kurt} slowly reduces as the tool wear progresses. This negative gradient indicates the DCB is wearing into a more circular form, leading to more

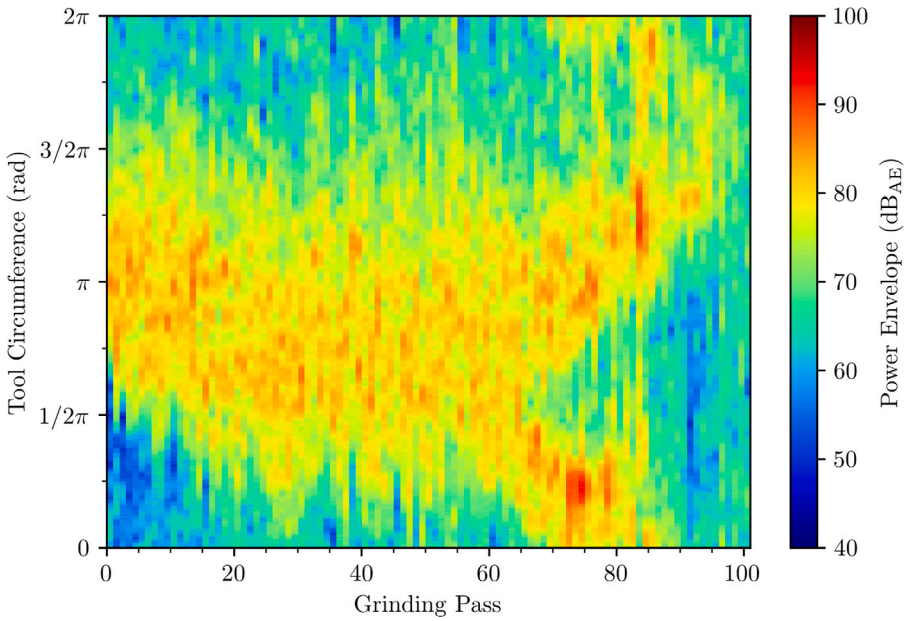

Fig. 19. AE power envelope from a single tool revolution of every grinding pass during test 8.

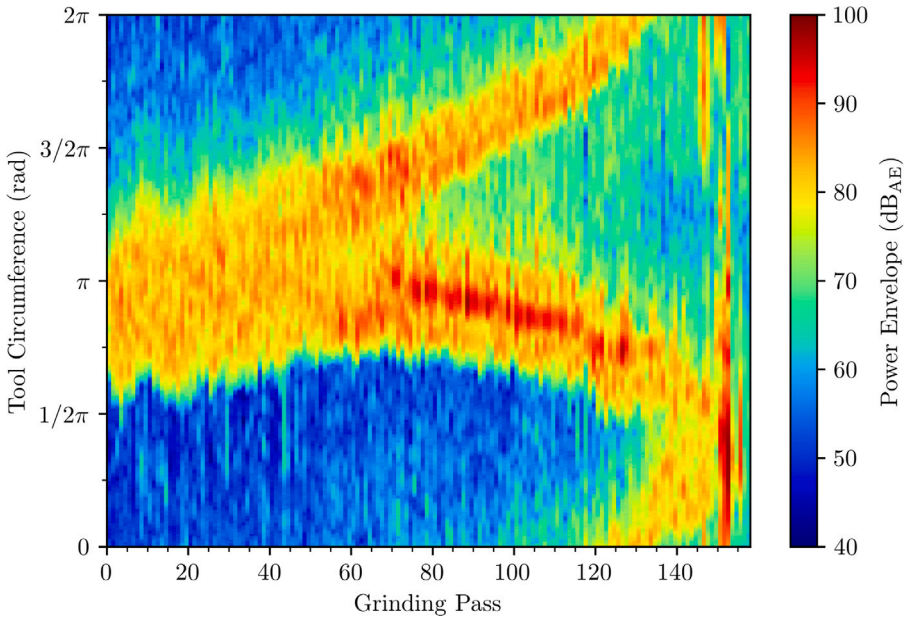

Fig. 20. AE power envelope from a single tool revolution of every grinding pass during test 10.

consistent workpiece contact and AE generation. Whilst this is more apparent for DCBs with higher runout, in tests 8 and 10, it is still observed for DCBs with low runout, such as in test 4. The minimum AE_{kurt} occurs during grinding pass 109, 67 and 52 for tests 4, 8 and 10 respectively, after which the AE_{kurt} suddenly increases and becomes more erratic in nature. These transition points align with the formation of craters and wear of the initial high spot on each DCB's surface. The following rise in AE_{kurt} increases in scale with the level of runout. Increases in AE_{kurt} are compounded when the DCB has a high level of runout, as it both forms peaks that are more prominent and cover a smaller proportion of the DCB's circumference, leading to the generation of higher amplitude AE over much smaller time periods. Both of which increase the "tailedness" of the AE distribution, in turn increasing the AE_{kurt}. As a result, after surface craters have been formed, the effect of a DCB's runout on the AE_{kurt} is overshadowed by the dramatic increase in AE power over short time periods, dramatically increasing the amplitude of the AE distributions outliers. As such, AE_{kurt} can be seen as a very useful AE feature for predicting a DCB's runout level up until large scale wear on the tool's surface. However, potentially of greater use AE_{kurt} can be seen as an indicator of the formation of surface craters and large scale wear across the entire DCB's length.

The AE_{RMS} represents the energy present within a continuous AE signal, making it a good indicator for the level of grinding contact between a wheel and workpiece. As such, AE_{RMS} has been used extensively for detecting the contact period and measuring wheel wear [31, 44,45]. Similarly to the AE_{kurt} in Fig. 22, the wear-in phase of each tool can be identified through the initial variation in AE_{RMS} prior to settling at a steady baseline shown in Fig. 21. Fig. 21 shows that once through the wear-in phase DCBs with low runout, such as in test 4, produce a consistent but high level of AE_{RMS}, until reaching the wear-out phase. In contrast, the DCBs from test 8 and 10 produce a lower level of AE_{RMS} throughout their steady-state phases. In order for the

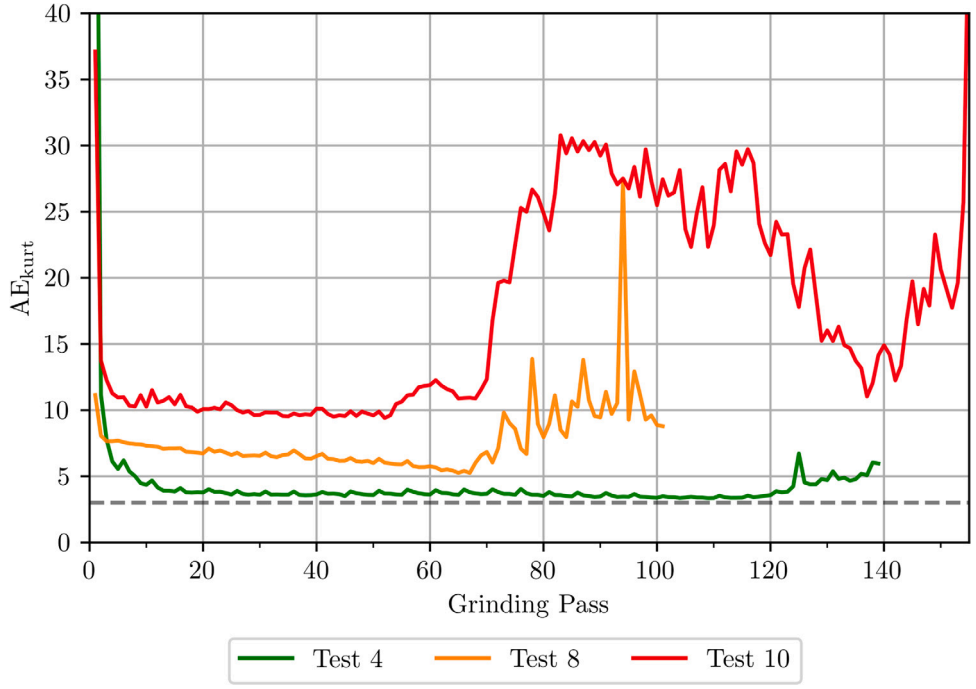

Fig. 21. AE_{RMS} throughout tests 4, 8 and 10.

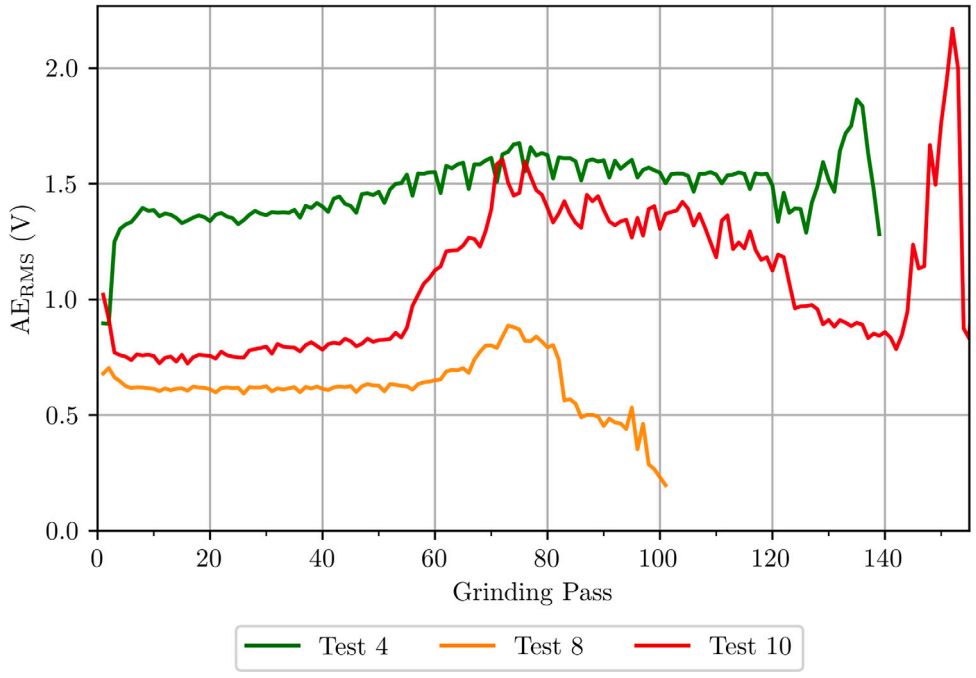

Fig. 22. AE_{kurt} throughout tests 4, 8 and 10.

AE_{RMS} to increase, either the maximum AE amplitude or the duration held at that level must increase. Resulting in the more consistent level of grinding produced by "low" runout tools, yielding higher levels of AE_{RMS}. With the reduction in tool-workpiece contact present during tests 8 and 10 explains the lowered level of AE_{RMS} in comparison to test 4. Once the high spot of the DCBs seen in tests 8 and 10 have worn through, the AE_{RMS} increases to a peak, the level of which indicating the scale/severity of the wear. The AE_{RMS} plots seen in Fig. 21 allow for an understanding of the DCB's wear progression, similar to the aligned AE power envelopes in Figs. 18–20. Fig. 21 verifies that AE_{RMS} is a capable indicator for the intensity of grinding over the entire workpiece's length. But without prior knowledge, it can be difficult to determine a given DCB's wear state.

Overall, AE can identify a given DCB's runout level through the changing contact between workpiece and tool. Through the sectioning and alignment of the time domain AE signals based on the rotational speed of the DCB, the severity of the high spot can be established, and its wear monitored, as seen in Fig. 20. Additionally, the use of averaging features such as AE_{kurt} and AE_{RMS} allows the tracking of each DCBs current state. Both features show the transition from the initial to steady-state wear phases, with AE_{kurt} being more sensitive to the tool's level of runout. Furthermore, AE is clearly effected by a DCB's runout

impacting both the amplitude and overall signal characteristics. When utilising a TCM approach based on AE the signal changes stemming from runout could lead to premature tool replacement, without the consideration of this effect, further increasing the existing tool-life wastage. However, these changes as a result of a tool's runout also potentially allow for an on-machine, indirect and passive sensing methodology of determining a DCB's runout and monitoring its wear simultaneously.

4. Conclusion

This paper has presented the effect runout plays on a DCB's overall life and wear mechanisms. As well as demonstrating the impact runout has on acquired AE signals throughout the grinding process, from which the runout level and wear state can be inferred. Twelve wear tests were conducted with constant grinding procedure and parameters, whereby a ⌀ 1.3 mm #1000 DCB was used to grind a SiC workpiece. Using an adjustable tool-holder, three different runout ranges were investigated, during which frequent on-machine tool wear measurements and continuous AE were acquired. A decrease in total useable life of a DCB and an increased variability were established as a result of increasing initial runout levels. Each DCB followed the traditional three-phase wear cycle, which was monitored through in situ 2D tool wear measurements. A novel use of a NC4 laser tool setter allowed full-field tool surface measurements to be taken within the machine tool, showing the difference in overall wear mechanisms between DCBs with "high" and "low" levels of runout. AE time-domain signals, acquired during the grinding period, clearly showed the effect of increasing runout through the fluctuating AE power levels over a single DCB rotation. Through the alignment of AE power envelopes, the wear of a DCB's high spot can be observed and tracked around its circumference. Additionally, simpler AE features extracted during the grinding period were investigated as wear indicators. Both AE_{kurt} and AE_{RMS} showed promise as wear indicators, being able to identify the transition from initial to steady-state wear phases across all investigated runout ranges. Additionally, the magnitude of AE_{kurt} generated by a given DCB once worn-in, indicated the severity of its runout level. AE_{kurt} slowly decreased during a tool's steady-state region suggesting the DCB is wearing into true form, furthermore abrupt increases in AE_{kurt} were seen to align with the formation of a large surface crater on the DCB's surface, across which the entire abrasive layer has been removed. This work adds further information into both the wear of DCBs in more representative scenarios whereby runout is considered, and the effect this has on AE as a promising TCM sensing method. As well as presenting the benefit of using an indirect method to detect the presence of excessive runout allowing a reduction in cost and wastage from the imperfect currently deployed TCM approaches.

CRediT authorship contribution statement

Thomas Jessel: Writing – original draft, Visualization, Methodology, Investigation, Formal analysis, Data curation, Conceptualization. **Carl Byrne:** Writing – review & editing, Supervision, Conceptualization. **Mark Eaton:** Writing – review & editing, Supervision, Conceptualization. **Ben Merrifield:** Writing – review & editing, Supervision, Methodology, Conceptualization. **Rhys Pullin:** Writing – review & editing, Supervision, Funding acquisition, Conceptualization.

Funding

This work was funded by an ESPRC iCASE award in partnership with Renishaw plc.

Declaration of competing interest

The authors declare that they have no known competing financial interests or personal relationships that could have appeared to influence the work reported in this paper.

Acknowledgements

All authors read and approved the final manuscript.

Data availability

Data will be made available on request.

References

[1] I.D. Marinescu, M. Hitchiner, E. Uhlmann, W.B. Rowe, I. Inasaki, Handbook of Machining with Grinding Wheels, Manufacturing Engineering And Materials Processing, Taylor & Francis Group, 2007.
[2] Z. Valdez-Nava, D. Kenfaui, M.-L. Locatelli, L. Laudebat, S. Guillemet, Ceramic substrates for high voltage power electronics: Past, present and future, in: 2019 IEEE International Workshop on Integrated Power Packaging, IWIPP, 2019, pp. 91–96, http://dx.doi.org/10.1109/IWIPP.2019.8799084.
[3] H. Matsunami, Fundamental research on semiconductor SiC and its applications to power electronics, Proc. Japan Acad. Ser. B 96 (7) (2020) 235–254, http://dx.doi.org/10.2183/pjab.96.018.
[4] X.-F. Song, H.-T. Ren, L. Yin, Machinability of lithium disilicate glass ceramic in in vitro dental diamond bur adjusting process, J. Mech. Behav. Biomed. Mater. 53 (2016) 78–92, http://dx.doi.org/10.1016/j.jmbbm.2015.08.003.
[5] J. Kelly, P. Benetti, Ceramic materials in dentistry: Historical evolution and current practice, Aust. Dent. J. 56 (s1) (2011) 84–96, http://dx.doi.org/10.1111/j.1834-7819.2010.01299.x.
[6] T. Ayode Otitoju, P. Ugochukwu Okoye, G. Chen, Y. Li, M. Onyeka Okoye, S. Li, Advanced ceramic components: Materials, fabrication, and applications, J. Ind. Eng. Chem. 85 (2020) 34–65, http://dx.doi.org/10.1016/j.jiec.2020.02.002.
[7] W. König, L. Cronjäger, G. Spur, H.K. Tönshoff, M. Vigneau, W.J. Zdeblick, Machining of new materials, CIRP Ann 39 (2) (1990) 673–681, http://dx.doi.org/10.1016/S0007-8506(07)63004-2.
[8] A. Choudhary, S. Paul, The wear mechanisms of diamond grits in grinding of alumina and yttria-stabilized zirconia under different cooling-lubrication schemes, Wear 454–455 (2020) 203315, http://dx.doi.org/10.1016/j.wear.2020.203315.
[9] L.E.A. Sanchez, J.F.G. Oliveira, R.T. Coelho, Detection of cracks in scratching tests in ceramic materials through acoustic emission, Proc. Inst. Mech. Eng. Part B 219 (9) (2005) 685–693, http://dx.doi.org/10.1243/095440505X32616.
[10] D.Y. Pimenov, L.R.R. da Silva, A. Ercetin, O. Der, T. Mikolajczyk, K. Giasin, State-of-the-art review of applications of image processing techniques for tool condition monitoring on conventional machining processes, Int. J. Adv. Manuf. Technol. 130 (1) (2024) 57–85, http://dx.doi.org/10.1007/s00170-023-12679-1.
[11] J. Liu, C. Jiang, X. Yang, S. Sun, Review of the application of acoustic emission technology in green manufacturing, Int. J. Precis. Eng. Manuf.-Green Technol. 11 (3) (2024) 995–1016, http://dx.doi.org/10.1007/s40684-023-00557-w.
[12] N. Pietrow, D. Curtis, D. Novovic, J. McGourlay, H. Ghadbeigi, Evolution of electroplated cubic boron nitride tool surface texture parameters during point grinding, J. Manuf. Sci. Eng. 144 (121007) (2022) http://dx.doi.org/10.1115/1.4054990.
[13] Z. Shi, S. Malkin, Wear of electroplated CBN grinding wheels, J. Manuf. Sci. Eng. 128 (1) (2005) 110–118, http://dx.doi.org/10.1115/1.2122987.
[14] W.B. Rowe, 4 - grinding wheel dressing, in: W.B. Rowe (Ed.), Principles of Modern Grinding Technology (Second Edition), William Andrew Publishing, Oxford, 2014, pp. 63–82, http://dx.doi.org/10.1016/B978-0-323-24271-4.00004-X.
[15] X. Zhang, K.F. Ehmann, T. Yu, W. Wang, Cutting forces in micro-end-milling processes, Int. J. Mach. Tools Manuf. 107 (2016) 21–40, http://dx.doi.org/10.1016/j.ijmachtools.2016.04.012.
[16] E. Diez, H. Perez, M. Guzman, A. Vizan, An improved methodology for the experimental evaluation of tool runout in peripheral milling, Int. J. Adv. Manuf. Technol. 65 (1) (2013) 283–293, http://dx.doi.org/10.1007/s00170-012-4168-2.
[17] C. Feng, Z. Cui, Y. Zhang, T. Yang, Electroplating technology of suspended diamond particles surface based on rotating electrode, Diam. Relat. Mater. 128 (2022) 109270, http://dx.doi.org/10.1016/j.diamond.2022.109270.
[18] A. Attanasio, Tool run-out measurement in micro milling, Micromachines 8 (7) (2017) http://dx.doi.org/10.3390/mi8070221.
[19] J. Badger, S. Murphy, G. O'Donnell, The effect of wheel eccentricity and run-out on grinding forces, waviness, wheel wear and chatter, Int. J. Mach. Tools Manuf. 51 (10) (2011) 766–774, http://dx.doi.org/10.1016/j.ijmachtools.2011.06.006.
[20] J. Baumann, T. Siebrecht, P. Wiederkehr, D. Biermann, The effect of runout errors on process forces and tool wear, Procedia CIRP 79 (2019) 39–44, http://dx.doi.org/10.1016/j.procir.2019.02.008.
[21] K. Li, K. Zhu, T. Mei, A generic instantaneous undeformed chip thickness model for the cutting force modeling in micromilling, Int. J. Mach. Tools Manuf. 105 (2016) 23–31, http://dx.doi.org/10.1016/j.ijmachtools.2016.03.002.

[22] J.A. Couey, E.R. Marsh, B.R. Knapp, R.R. Vallance, In-process force monitoring for precision grinding semiconductor silicon wafers, Int. J. Manuf. Technol. Manag. 7 (5–6) (2005) 430–440, http://dx.doi.org/10.1504/IJMTM.2005.007695.

[23] T.W. Hwang, C.J. Evans, S. Malkin, High speed grinding of silicon nitride with electroplated diamond wheels, part 2: Wheel topography and grinding mechanisms, J. Manuf. Sci. Eng. 122 (1) (1999) 42–50, http://dx.doi.org/10.1115/1.538909.

[24] A. Gouarir, G. Martínez-Arellano, G. Terrazas, P. Benardos, S. Ratchev, In-process tool wear prediction system based on machine learning techniques and force analysis, Procedia CIRP 77 (2018) 501–504, http://dx.doi.org/10.1016/j.procir.2018.08.253.

[25] E. Sauter, E. Sarikaya, M. Winter, K. Wegener, In-process detection of grinding burn using machine learning, Int. J. Adv. Manuf. Technol. 115 (7–8) (2021) 2281–2297, http://dx.doi.org/10.1007/s00170-021-06896-9.

[26] E. Brazel, R. Hanley, G.E. O'Donnell, The effects of process parameters on spindle power consumption in abrasive machining of CoCr alloy, J. Mach. Eng. 11 (4) (2011) 59–69.

[27] M. Hacksteiner, H. Peherstorfer, F. Bleicher, Energy efficiency of state-of-the-art grinding processes, Procedia Manuf. 21 (2018) 717–724, http://dx.doi.org/10.1016/j.promfg.2018.02.176.

[28] Y. Wang, J. Xiang, R. Markert, M. Liang, Spectral kurtosis for fault detection, diagnosis and prognostics of rotating machines: A review with applications, Mech. Syst. Signal Process. 66–67 (2016) 679–698, http://dx.doi.org/10.1016/j.ymssp.2015.04.039.

[29] M. Shah, V. Vakharia, R. Chaudhari, J. Vora, D.Y. Pimenov, K. Giasin, Tool wear prediction in face milling of stainless steel using singular generative adversarial network and LSTM deep learning models, Int. J. Adv. Manuf. Technol. 121 (1) (2022) 723–736, http://dx.doi.org/10.1007/s00170-022-09356-0.

[30] V.H. Nguyen, T.H. Vuong, Q.T. Nguyen, Feature representation of audible sound signal in monitoring surface roughness of the grinding process, Prod. Manuf. Res. 10 (1) (2022) 606–623, http://dx.doi.org/10.1080/21693277.2022.2108927.

[31] J. Webster, W.P. Dong, R. Lindsay, Raw acoustic emission signal analysis of grinding process, CIRP Ann 45 (1) (1996) 335–340, http://dx.doi.org/10.1016/S0007-8506(07)63075-3.

[32] L. Wan, X. Zhang, Q. Zhou, D. Wen, X. Ran, Acoustic emission identification of wheel wear states in engineering ceramic grinding based on parameter-adaptive VMD, Ceram. Int. 49 (9, Part A) (2023) 13618–13630, http://dx.doi.org/10.1016/j.ceramint.2022.12.238.

[33] I. Yesilyurt, A. Dalkiran, O. Yesil, O. Mustak, Scalogram-based instantaneous features of acoustic emission in grinding burn detection, J. Dyn. Monit. Diagn. 1 (1) (2022) 19–28, http://dx.doi.org/10.37965/jdmd.2021.49.

[34] W. Huang, Y. Li, X. Wu, J. Shen, The wear detection of mill-grinding tool based on acoustic emission sensor, Int. J. Adv. Manuf. Technol. 124 (11) (2023) 4121–4130, http://dx.doi.org/10.1007/s00170-022-09058-7.

[35] Z. Liu, B. Chen, H. Xu, G. Liu, W. Ou, J. Wu, A study of diamond grinding wheel wear condition monitoring based on acoustic emission signals, Int. J. Adv. Manuf. Technol. 134 (9) (2024) 4367–4385, http://dx.doi.org/10.1007/s00170-024-14392-z.

[36] T. Jessel, C. Byrne, M. Eaton, B. Merrifield, S. Harris, R. Pullin, Tool condition monitoring of diamond-coated burrs with acoustic emission utilising machine learning methods, Int. J. Adv. Manuf. Technol. 130 (3) (2024) 1107–1124, http://dx.doi.org/10.1007/s00170-023-12700-7.

[37] Nikken-World, Zero-Fit, [online, cited 2025-03-18].

[38] Y.-C. Chen, P.-Z. Chang, Y.-C. Tsai, Runout parameters identification in milling process, Procedia CIRP 130 (2024) 656–661, http://dx.doi.org/10.1016/j.procir.2024.10.144.

[39] N. Pietrow, D. Curtis, H. Ghadbeigi, D. Novovic, J. McGourlay, An investigation into the challenges of the point grinding machining process, Procedia CIRP 101 (2021) 190–193, http://dx.doi.org/10.1016/j.procir.2020.09.195.

[40] Renishaw plc, Renishaw: NC4, [online, cited 2022-04-20].

[41] Renishaw plc, White Paper: Innovative Laser Tool Setting Technology Provides Accuracy, Flexibility and Robust Operation, [online, cited 2025-06-02].

[42] Renishaw plc, Understanding non-contact tool setting, 2003.

[43] T. Jessel, C. Byrne, M.J. Eaton, R. Pullin, The capability of acoustic emission features to monitor diamond-coated burr grinding wear and effectiveness, E-J. Nondestruct. Test. 29 (10) (2024) http://dx.doi.org/10.58286/30231.

[44] D.E. Lee, I. Hwang, C.M.O. Valente, J.F.G. Oliveira, D.A. Dornfeld, Precision manufacturing process monitoring with acoustic emission, in: L. Wang, R.X. Gao (Eds.), Condition Monitoring and Control for Intelligent Manufacturing, in: Springer Series in Advanced Manufacturing, Springer, London, 2006, pp. 33–54, http://dx.doi.org/10.1007/1-84628-269-1_2.

[45] C.-H. Shen, Acoustic emission based grinding wheel wear monitoring: Signal processing and feature extraction, Appl. Acoust. 196 (2022) 108863, http://dx.doi.org/10.1016/j.apacoust.2022.108863.